JOURNAL OF PROPULSION AND POWER
Vol. 25, No. 3, May–June 2009

Flame-Spreading Behavior in a Fin-Slot Solid Rocket Motor Grain (Part II)

Jeffrey D. Moore,* Kenneth K. Kuo,† and Peter J. Ferrara‡
Pennsylvania State University, University Park, Pennsylvania 16802

DOI: 10.2514/1.38166

To accurately predict the overall ignition transient for the reusable solid rocket motors of the space shuttle booster with head-end fin slots, it is necessary to have the knowledge of the flame-spreading rates in the fin-slot region. This paper is the second of a two part study and deals with the development of a flame-spreading correlation in the fin-slot region. A subscale (1:10) pie-shaped fin-slot motor was designed to perform diagnostic measurements for studying the flame-spreading behavior on the exposed propellant surface. Dynamic similarity was considered in the igniter design so the impinging jet had a similar exit angle onto the propellant surface in the fin-slot section. Flame-spreading measurements were gathered using a high-speed digital camera and nonintrusive optical measurement methods through an array of 36 near-infrared fast-response photodetectors installed perpendicular to representative regions of the propellant surface. Results showed that the flame-spreading phenomena was highly nonuniform, starting in the downstream portion of the fin-slot region before traveling back toward the igniter. A correlation was developed for the dimensionless flame-spreading time interval showing that it was inversely proportional to the pressurization rate to a power of 0.62, which depends strongly upon the flow parameters of the igniter induced flow and local propellant grain geometry.

Nomenclature

A	=	burnt propellant surface area
C	=	constant in the empirical flame-spreading correlation
L	=	length of the curved flame front
$\bar{L}$	=	average length of the curved flame front
n	=	exponent in the empirical flame-spreading correlation
P	=	instantaneous chamber pressure
t	=	time
V	=	velocity of the gas mixture or flame front
τ	=	dimensionless time

Subscripts

core	=	igniter core flow
res	=	residence

I. Introduction

IN THE area of solid propellant rockets, numerous researchers have studied the flame-spreading processes, flowfield structures, and ignition transients using a variety of laboratory-scale motors [1–5]. Despite the abundant research, limited work on flowfield structure, heat-transfer rates, and flame spreading have been conducted in more complex propellant grain geometries, like propellant grains with fin slots in solid rocket motors. There has been some recent computational [5,6] and experimental [7] work performed in the aft-end fin slots and computational flame-spreading studies of head-end fin slots [8]. Applications for these complex grains can be directly seen in the space shuttle rocket booster, where the head-end fin-slot region acts as one of the four booster segments [9]. A major reason behind the incorporation of fin slots in the space shuttle booster design is the benefit of the large propellant burning surface area of the fin-slot region, which provides a high amount of thrust in a short amount of time, vital for the space shuttle liftoff [10–12]. Better understanding of the overall ignition transient is an important concern and requirement for efficient burning of a solid rocket motor [13], and it is the behavior of the igniter hot products and motor geometry that can have the most influential effect on the flame-spreading phenomena and the overall ignition transient [3]. Therefore, in order to improve the understanding of the flame-spreading phenomena in head-end propellant grains with fin slots, a series of igniter and propellant experiments were conducted in an approximately 1:10 scale reusable solid rocket motor (RSRM) to determine the dependency of flame-spreading processes on the igniter induced flowfield and associated heat-transfer rates inside the fin-slot region.

II. Research Objectives

To predict the flame-spreading process in the fin-slot region, the first step was to study the flowfield induced by the discharging of the igniter jet in the induction interval before the onset of ignition at certain locations on the exposed propellant surface, followed by flame spreading and chamber filling intervals [1,4,13,14]. It is in the induction interval that the igniter gas induced flowfield directly influences the heat-transfer processes and the subsequent ignition-front propagation in the flame-spreading interval. Essentially, the ignition delay and the flame-spreading pattern depend strongly on the energy transferred from the igniter products to the propellant surface [1,4,15]. Early indications of the fin-slot induced flowfield structure were observed through flow visualization methods by way of chalk/powder kerosene and fine threads applied to the test rig's acrylic sacrificial window [16]. These results showed a large recirculating field developed in the middle of the fin-slot region, with two small recirculating fields in the upper corners having opposite flow directions. These multiple recirculating flowfields helped to produce convection-dominated heat-transfer rates at different locations throughout the fin-slot region. The radiative energy transfer was less than 25% of the overall heat-transfer rates. Moore et al. [17] conducted tests with igniter flow into an inert fin-slot propellant region and showed multiple recirculating regions inside the fin slot

Presented as Paper 5780 at the 43rd AIAA/ASME/SAE/ASEE Joint Propulsion Conference and Exhibit, Cincinnati, OH, 8–11 July 2007; received 20 April 2008; accepted for publication 8 October 2008.

*Ph.D. Candidate, Department of Mechanical and Nuclear Engineering, 139 Research Building East. Student Member AIAA.

†Distinguished Professor, Department of Mechanical and Nuclear Engineering, 140 Research Building East. Fellow AIAA.

‡Research Assistant, Department of Mechanical and Nuclear Engineering, 139 Research Building East. Student Member AIAA.

with varying heat-transfer rates over the exposed propellant surface; their work resulted in a heat-transfer correlation in the fin-slot region.

The specific objectives for this investigation were 1) utilization of pyrogen igniter products for studying the flame-spreading process in the fin-slot section of the rocket motor simulator, 2) observation of the flame-spreading phenomena and measurements of the flame-spreading rates using several nonintrusive diagnostics techniques, and 3) analysis of experimental data to develop a correlation of the flame-spreading time interval in the head-end fin-slot region of the motor simulator.

III. Method of Approach

The study of the flame-spreading processes in the space shuttle RSRM was to be approached by using an approximately 1:10 scaled RSRM test rig. The test rig previously designed and operated to study the flame-spreading processes in an aft-end fin-slot solid rocket motor [7] was modified for this work. The existing motor housed a single, pie-shaped propellant holder, which was able to have space shuttle RSRM propellant samples cast on both sides, acting as the fin-slot region propellant. This pie-shape propellant holder represented one of the 11-point star-shaped fin slots of the actual RSRM, supplying these experiments with two fin-slot regions for diagnostic studies.

A. Experimental Fin-Slot Motor

The test rig consisted of seven major components: the main chamber for housing the propellant holder, a fin-slot propellant holder, a sacrificial inner acrylic window, an outer main viewing acrylic window, an exit nozzle, an igniter body and nozzle, and a 36 port diagnostic holder. For these experiments, each pyrogen igniter was initiated by a small pyrotechnic squib inserted into the igniter body [17]. Additional component details and images can be seen in a previous technical papers [16,17].

1. Main Fin-Slot Motor Test Rig Design

For this series of test runs, the main chamber exit nozzle was graphite with a constant diameter of 5.33 cm. A reason behind this large nozzle throat diameter was to prevent any large pressurization levels in the chamber. The igniter nozzle throat was also graphite and the diameter was set at 0.56 cm for all experiments. Both nozzles were examined after each test for erosion and replaced when needed. To maintain dynamic similarity to the actual RSRM, the igniter area expansion ratio was held at 1.83, the expansion angle equaled 27 deg, and the Reynolds number scaled accordingly to maintain turbulent flow. This was very important so that the exiting hot igniter products would impinge the fin-slot propellant surface in the corresponding location as that of the full-scale RSRM. Optical diagnostics, which are discussed later, were applied on one side to the fin-slot motor, replacing a pair of windows. On the opposite side of the motor, a pair of windows was used for high-speed video imaging. Lastly, the propellant was cast to the propellant holder at a constant web thickness of 0.5 cm; this thickness was sufficient to simulate the thermally thick propellant grain and minimize cold-end effects.

2. Diagnostic Methods

Because of the flame-spreading event across the propellant surface, a method was needed to determine where the flame-front position was over time. In a study performed by Thynell et al. [18], it was shown that optical signals from the ignited propellant surface could be differentiated from those of an unignited propellant surface, even in the presence of combustion product gases. The selection of infrared photodetectors was based upon three criteria: 1) measurement locations must have adequate optical access for detection, 2) energy emitted from the hot burning surface must be distinguishable from flowing combustion product gases, and 3) the measurement system must be able to record the rapidly changing event [18].

This was accomplished by using near-IR (infrared) PbSe photodetectors mounted on the 36-port diagnostic holder. The advantage of using near-IR photodetectors was that the wavelength range of detection was 1.5–4.0 μm and a response time of less than 10 μs. Therefore, a large change in voltage would be detected for propellant surface burning in front of the photodetectors, as opposed to a very small voltage change for the hot igniter products. From these voltage changes, the path of the flame-spreading phenomena could be determined and mapped out over time, meeting all three of the preceding outlined criteria.

Because the combustion event inside the fin-slot motor would reach temperatures above 2000 K, an assembly was constructed to protect the photodetectors from hot gas exposure, seen in Fig. 1. The assembly included a sacrificial and sapphire window inserted into a cavity that contained an o-ring in a groove. Beyond this groove was the photodetector. Therefore, the window was the only surface in contact with the burning propellant surface. Also, the sapphire window allowed over 85% transmission for the required photodetector wavelengths. To hold the window in place, a piece of metal was threaded tight against a ceramic spacer in contact with the window. The spacer and the metal had a small hole cut through the center to allow for light detection.

Besides having an array of photodetectors to detect the burning surface of the fin-slot propellant, a high-speed colored digital camera was used to visually capture the event. This all owed for the simultaneous monitoring of the flame-spreading event by having the diagnostic holder with photodetectors on one side of the fin-slot motor and a high-speed digital camera looking through the assembly of a sacrificial window and a main window located on the other side. Frame rates were set at 10,000 fps. The camera trigger was linked to the data acquisition systems to ensure all the diagnostics were synchronized to the exact same igniter trigger time. The visual images of the flame-spreading at each time step could then be compared with the other diagnostic data to develop the flame-spreading correlation.

The configuration of the diagnostic ports (using photodetectors or exposed thermocouples) at different locations on the diagnostic panel together with the igniter jet location is shown in Fig. 2. These gauges can be mounted interchangeably on the 36 ports of the diagnostic panel. The array of diagnostic ports was organized into five rows with each port being assigned a number. The length and height of the fin-slot region are 42.2 cm and 12.2 cm, respectively.

To determine the ignition delay at a specific diagnostic port location, the recorded photodetector signal was used with a "slope method." This method helped to define the first notable rise in voltage signal as the onset of the flame-spreading event. Maintaining consistency, the first rise of each gauge was determined by taking the intersection of the major slope increase with the baseline voltage.

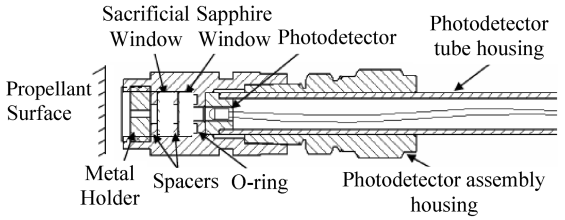

Fig. 1 Cross-sectional schematic of near-IR photodetector setup.

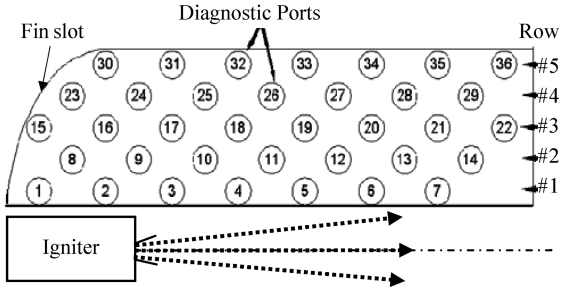

Fig. 2 Schematic of diagnostic holder ports and row orientation.

The onset of flame-spreading time defined in this manner differs only slightly from the time associated with the first discernable voltage rise from the trace. The actual time difference between these values is not significant in influencing the final result, as long as the same definition is used for all the photodetector gauges.

B. Flame-Spreading Correlation Development

The flame-spreading correlation was developed based on the combined data recorded from the fast-response near-IR photodetectors and high-speed digital camera images. Because all of the diagnostic data were directly linked to the same igniter squib triggering time as the high-speed digital camera, individual images from the test firing movie could be extracted at selected times throughout the test firing.

To examine the propellant surface burning condition closely, images were extracted at every 1 ms from the start of flame-spreading event. The flame-spreading start time was synchronized with the pressure-time (P-t) trace of the test firing in the fin-slot chamber and visual observation of the burning surface. In addition, photodetector data were used to verify ignition delay times.

To accurately deduce the high-speed digital camera images, a computer program was used. A LabVIEW program was developed as an image extractor, which used a combination of extracting specific colors at selected light threshold levels (0–255 maximum) to locate the propellant burning surface flame front. In total, eight fin-slot experiments were conducted. All of these experiments were conducted in the same manner. An example of this procedure from test 3 can be seen in Figs. 3a–3c.

A selected image was entered into the LabVIEW program (Fig. 3a). The image was then read and the light extracted to show the gray level distribution on the black and white image (Fig. 3b). From here, a manual threshold level was entered, highlighting the bright luminosity of the burning propellant surface and dark region for the unburnt region in the image equalization process (Fig. 3c). This figure also showed the detected states of burning at various photodetector locations. In the burnt region, the LabVIEW program was able to calculate the area and perimeter of the propellant burning surface in pixels. Depending on the image size (slightly different for each test due to camera alignment and cropping of the image to include fin-slot region only), an equation was used to convert the pixel area and length into metric units. This process was repeated for every image over the flame-spreading time period.

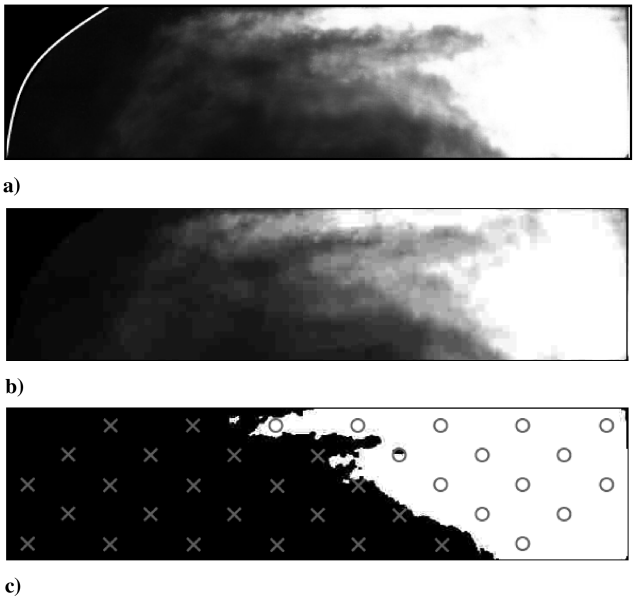

Fig. 3 Image extraction process from test 3 (at 0.037 s after the start of flame-spreading) with a) original high-speed image (white line was purposely added to represent the curved boundary of the fin-slot region), b) extracted high-speed image to show the gray level distribution, and c) extracted high-speed image with a selected threshold level for image equalization as a part of the image processing. The states of propellant burning at various locations determined from photodetector measurements are superimposed over the image (ignited shown by a gray circle and unignited shown by a gray x).

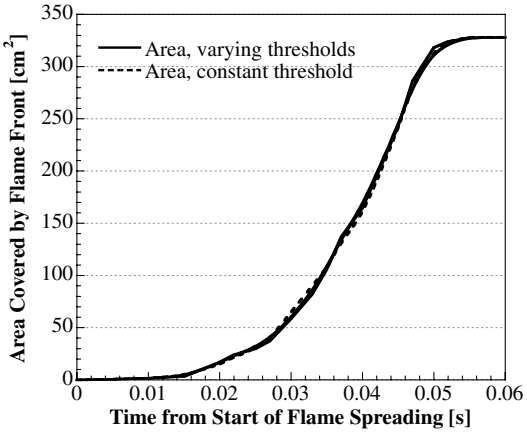

Fig. 4 Comparison of burned propellant surface area of test 3 using varying and constant threshold levels.

In the process of determining an adequate threshold level, the following comparison was made in order to ensure that the visually observed flame front with certain luminosity can be properly selected as the boundary for the burned propellant region. Various threshold levels for test 3 of the burning surface area at each selected time were plotted vs the burning surface area from the same test run using a constant threshold level. This comparison can be seen in Fig. 4. It was determined from this comparison that there was minimal difference in the measured burning surface areas (~6.8%). Therefore, to maintain consistency, a constant threshold level was selected for each test firing to calculate the burning surface area and the perimeter of the flame front.

To calculate the average flame-spreading velocity, the rate of change of burning surface area and the average length of the traveling flame front (FF) were needed. They are related to the average flame-spreading (FS) velocity by the following equation:

$$V_{\mathrm{FS}}(t) = \frac{1}{\bar{L}_{\mathrm{FF}}(t)} \frac{\mathrm{d}A}{\mathrm{d}t} \tag{1}$$

To obtain the time derivative of the propellant burning surface area, the instantaneous surface area determined from LabVIEW was fitted to a fourth-order polynomial and then differentiated. The expression for this derivative was divided by the average length of the instantaneous flame front, which was calculated by taking the flame-front length between two selected time steps.

The flame-front length was then determined by taking the average length between two time steps ($n + 1$ and n) in the flame-spreading region as follows:

$$\bar{L}_{\mathrm{FF}}(t) = \frac{L_{n+1} + L_n}{2} \tag{2}$$

where L_{n+1} and L_n are the instantaneous length of the curved flame fronts at times t_{n+1} and t_n, respectively. These two parameters were determined through the use of the LabVIEW program.

IV. Discussion and Results

Results of the fin-slot chamber pressure for all eight fin-slot tests can be seen in Fig. 5. The igniter event was roughly 0.3 s in duration. Even though variation can sometimes occur between motor peak pressures with same pyrogen igniter for actual RSRM flights, as one can see, the slopes of the pressure curves and overall pressure profiles of all eight fin-slot tests matched very well, especially in the region for $t < 0.75$ s, including where flame-spreading occurred.

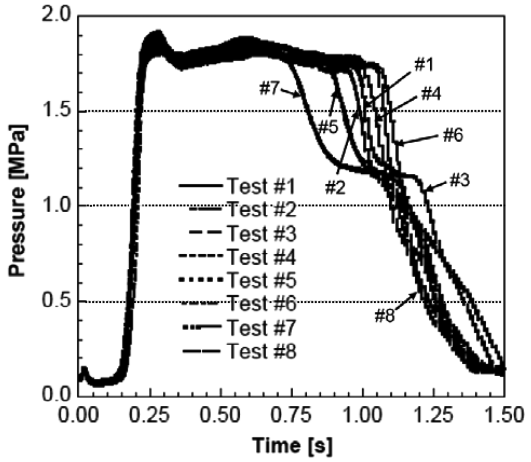

Fig. 5 Recorded main chamber *P-t* traces from the eight fin-slot propellant firings.

The average fin-slot chamber pressure was around 1.79 MPa and showed good reproducibility.

From the start of the igniter burning, overall test burn time was somewhere between 1.0 and 1.2 s. The difference in the *P-t* traces during the later phase of the combustion event could be attributed to the differences in the fin-web thickness around the propellant sample holder (some variations because propellant samples were cast from multiple propellant molds). Any increase or decrease in the propellant web thickness can contribute to the free volume of the motor, hence affecting the chamber pressure. However, these web thickness differences do not affect the results in the important time period, which is before $t = 0.21$ s. It is useful to note that the pressure levels reached during the tests we very close to that predicted by a volume filling code (∼1.72 MPa), which meant that the selected igniter and exit nozzles were acceptable for recreating the pressure levels needed in the lab-scale fin-slot motor to simulate the pressurization rate seen in the RSRM.

As mentioned previously, an important parameter considered in simulating the actual RSRM was closely simulating the pressurization rate. When compared with an actual RSRM head-end pressure trace, the pressure profiles from the motor simulator agreed rather well. The slopes of all eight fin-test firings appear to be very similar to that of the actual RSRM. The high reproducibility of the pressurization rates in the Pennsylvania State University's fin-slot motor simulator was demonstrated. Also, the entire flame-spreading event was completed during this pressurization interval. A more detailed comparison of the dP/dt for the eight propellant fin-slot tests and the actual RSRM can be seen in Figs. 6a and 6b.

Peak pressurization rate values for the eight fin-slot tests were very close in value, ranging from 34.5–41.4 MPa/s. Differences in these values and rise times can either be attributed to difference in the igniter propellant grains or slight differences in igniter nozzle throat diameter and rocket motor exit nozzle throat diameter. Each test was replaced with a new igniter nozzle. However, only three rocket motor exit nozzles were used in this study, and so some tests had the same exit nozzle. These nozzles showed nearly negligible erosion effects, which could cause a minor decrease in the pressurization rate of the motor. When compared with the actual RSRM data for the important flame-spreading period, the flame-spreading durations of the eight propellant fin-slot motor tests were in the same range as the RSRM test value (∼0.08 s).

Results from the photodetector and exposed fine-wire thermocouple signals showed that, similar to the igniter experiment results on the inert fin propellant surface [17], the photodetector traces showed varying ignition delay times at different locations on the propellant surface over the course of the flame-spreading event. These times were recorded and compared with the high-speed movie camera images (see Fig. 3c) to help develop a flame-spreading correlation in the fin-slot region.

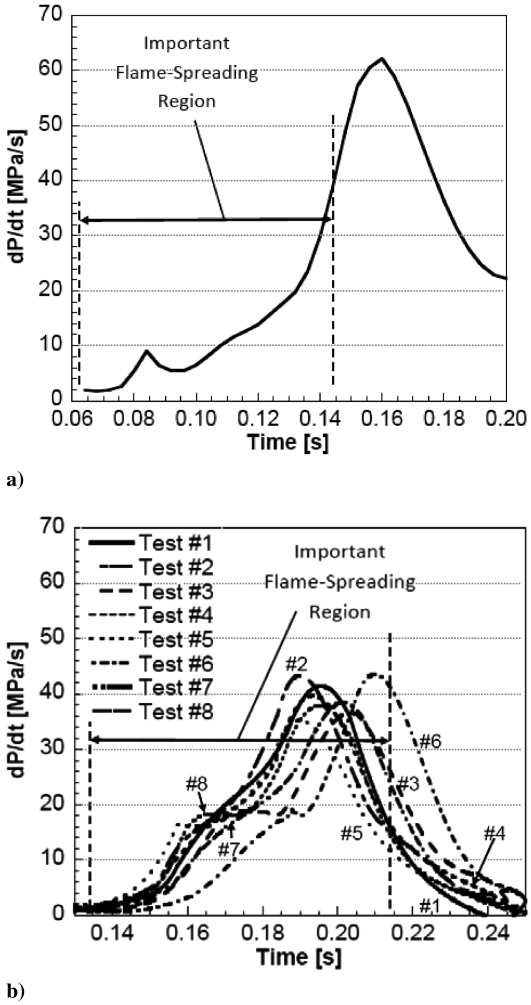

Fig. 6 Comparison of dP/dt for a) actual RSRM firing and b) eight fin-slot propellant tests.

A. Flame-Spreading Correlation

After all of the eight fin-slot experiments were completed, the high-speed digital camera images were analyzed and deduced in combination with all the diagnostic data. From these high-speed camera images, it was easy to visually identify the overall flame-spreading trends between the tests. As discussed earlier in the development of the flame-spreading correlation, the high-speed images were broken down into individual images 1 ms in time. Progression of the flame-spreading phenomena over a time of 55 ms can be seen in the images deduced from test 3 (see Figs. 7a–7e). The image times correspond to the start of ignition of the igniter propellant (or triggering signal). The configuration of the diagnostic port locations are included.

Based upon the high-speed images recorded from test 3, fin-slot ignition starts somewhere below and downstream of port 7 (Figs. 7a and 7b, ∼145–150 ms). This region was the portion of the propellant surface that was closest to the downstream cylindrical bore section. Governed by the counterclockwise recirculating flow (because igniter core flow was left to right), the region near ports 32–34 starts burning (Fig. 7c) due to a combination of hot gas impingement above port 33 and a thin flame corridor connecting the region around port 33 and port 7, due to igniter induced flow.

At this point, it is useful to mention that radiative effects were not important in the fin-slot tests. Because the edge region of the propellant sample had a greater view factor than that of the major portion of the propellant surface in the fin-slot region, it was expected that this entire propellant edge region would ignite first, if the radiation was important. However, this was not the case, because only a small region was ignited around port 33 due to flow impingement generated from the igniter products.

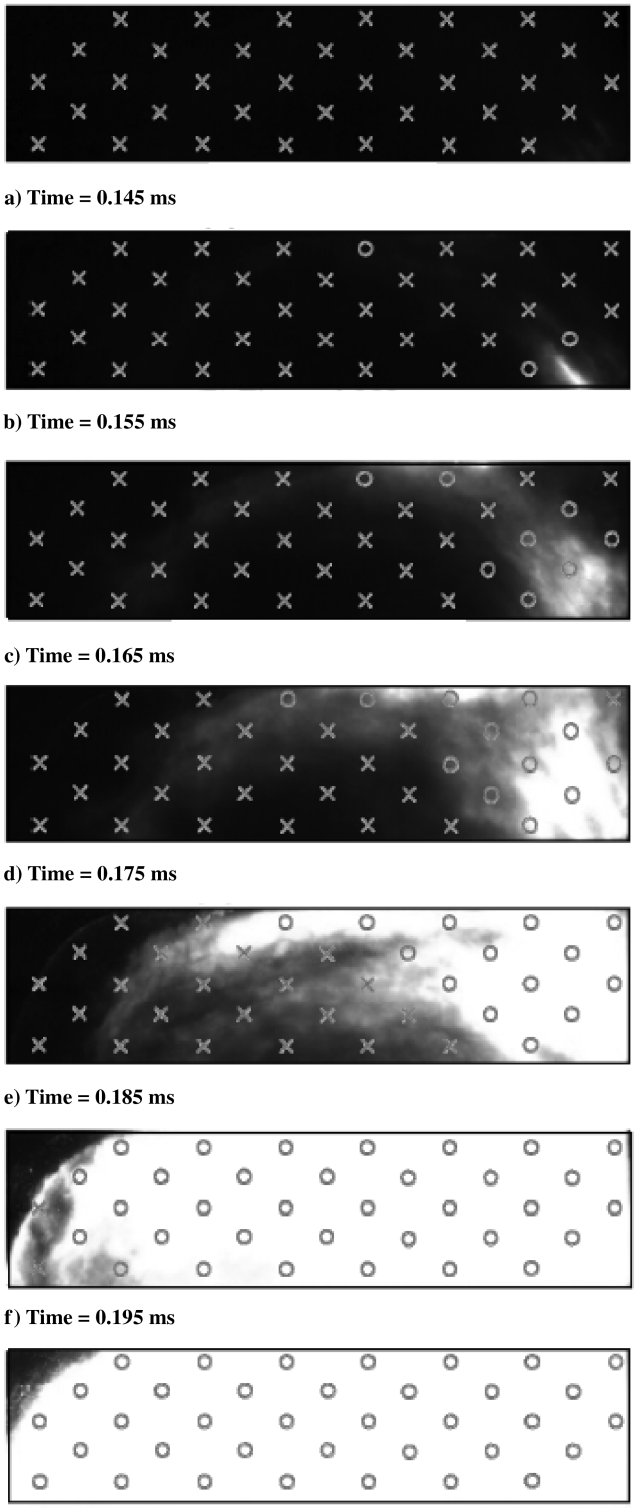

a) Time = 0.145 ms

b) Time = 0.155 ms

c) Time = 0.165 ms

d) Time = 0.175 ms

e) Time = 0.185 ms

f) Time = 0.195 ms

g) Time = 0.200 ms

Fig. 7 A set of high-speed digital images showing the flame-spreading event from test 3. The states of propellant burning at various locations determined from photodetector measurements are superimposed over some of the images (ignited shown by a gray circle and unignited shown by a gray x).

Although port 33 does not appear to display any burning in Figs. 7a and 7b, this location was always one of the first to show any change in temperature or voltage by the heat-flux and photodetector diagnostics for the eight fin-slot propellant tests. Flame spreading from these two regions (ports 7 and 33) join and expand in the surrounding ports 32, 34, 26, 27, 28, 29, 19, 20, 21, 22, 12, 13, 14, and 6 over time, creating a large burning area of the fin-slot propellant in the downstream section of the fin-slot region (Figs. 7d and 7e). The flame front continued to spread back toward the igniter end (up to Fig. 7f), noticeably following the path of the large counterclockwise portion that was seen in the igniter induced flow. By the time the main chamber pressure reached a maximum peak and quasi-steady pressure condition, the entire fin-slot region was ignited (Fig. 7g).

The fin-slot propellant continued to burn until the pressure decreased after around 1.0 to 1.2 s, where the light intensity began to diminish and the remaining burning section was observed to be the fin curvature portion.

The ignition delay data deduced from photodetector traces showed very good agreement with the observed flame-spreading phenomena based upon the high-speed video data discussed previously. The difference in the two diagnostic methods was that because the photodetectors detect only in the near-IR wavelength even with flowing combustion products as the media, the ignition delay of the ports with photodetectors were slightly earlier than visible light observation in the high-speed digital camera images. This was because the visible high-luminosity light was generated not only from the ignition of the propellant surface but also caused by the resultant hot propellant product gases flowing over the fin-slot surface. In certain cases, when signals in the near-IR wavelength range was received by the photodetectors, corresponding to the onset of initial propellant ignition and surface burning, the high-speed digital camera images at the same time did not display a notable image at the corresponding port location. Therefore, when determining the ignition delay, the traces recorded by the photodetectors and the high-speed digital camera images were examined together to achieve a more precise description of the flame-spreading event.

The high-speed digital images were imported into the LabVIEW image extractor program for determination of the instantaneous burning surface area, flame-front perimeter, and the length of curved flame front. Plots of burned area and flame-spreading velocity from selected test firings were created and are shown in Figs. 8a and 8b. It is interesting to note that the general trend of the burnt propellant surface area and flame-spreading velocities of these selected tests are reasonable and rational.

Initially, the flame-spreading rate starts out slowly, then as more area is burnt it gains speed during the final one-third of the flame-spreading interval, before decreasing in flame-spreading velocity near the end of the event. Typical maximum velocities in this fin-slot region were between 3.5–5.0 m/s, which is far below the flame-spreading rates in the circular-bore section, which can reach upwards of several hundred meters per second [9,19]. The large difference in flame-spreading velocities between these two regions is important, for it shows how the fin-slot region drives the overall ignition transient of the entire motor. The slower burning fin-slot region will ignite first, resulting initially in a somewhat neutral burn (thrust). Without any slots to enter, the progressive burning grains of the remaining segments will be influenced directly by the high velocity core flow inside the motor, increasing the shear and heating of the bore section grains.

Similar to the results seen in the aft-end fin-slot motor [7], it appears that the overall ignition transient processes in a solid rocket motor with head-end fin slots can also be rate-limited by the relatively slow flame-spreading phenomena in the fin-slot region. Depending upon the rocket motor design, flame-spreading velocities in the head-end fin-slot region can also be lower than those in the aft-end fin-slot region. In the fore-end fin-slot region, the flame-spreading process is governed by the discharging process of the hot igniter product jet, while in the aft-end fin-slot region the flame-spreading process depends upon the flow of the combustion products generated from the circular bore section and the contour of the submerged nozzle [7].

Because the igniter mass flow rates and fin-slot chamber pressure differed only slightly, the dP/dt profiles of the preceding tests were compared with the burnt propellant surface area over the flame-spreading interval and plotted in Fig. 9. There are three different levels of the total burnt surface area due to the alignment of the high-speed video camera with the propellant surface. By carefully

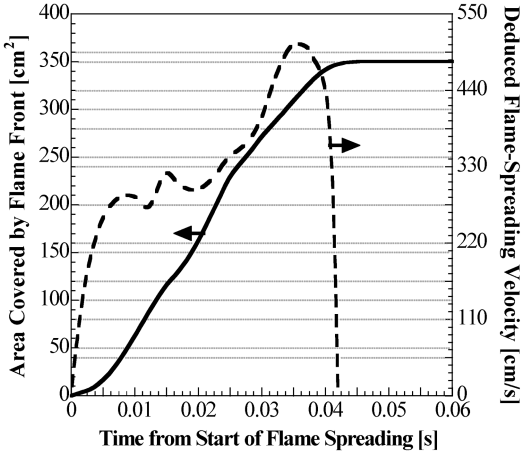

Fig. 8 Deduced instantaneous burnt propellant surface area and flame-spreading rates in the fin-slot region for a) test 1 and b) test 3.

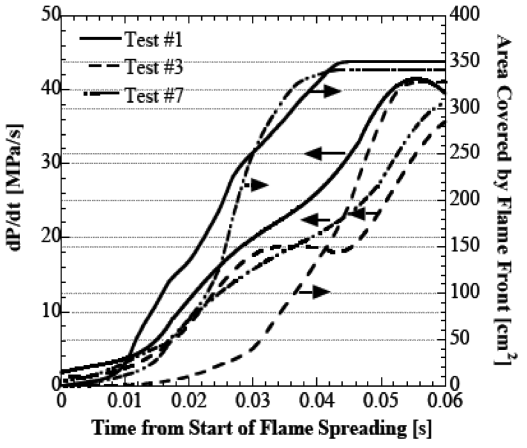

Fig. 9 Comparison of dP/dt and burnt propellant surface area in the fin-slot region for tests 1, 3, and 7.

examining the trend exhibited in this plot, it was observed that test 1 had the highest dP/dt over the flame-spreading interval. For test 1 the overall flame-spreading event over the entire propellant surface was completed the earliest. Tests 3 and 7 had similar pressurization rates in the early portion of the flame spreading; however, test 3 reached a plateau and had lower pressurization rates over the final one-third of the flame-spreading interval. This decrease in pressurization rate resulted in much slower flame-spreading process for test 3. It took the longest time for the flame to spread in comparison with both test 7 and 1. These three tests were selected because the high-speed digital camera images were the most clear for the demonstration of this strong relationship between the chamber pressurization rate and flame-spreading rate.

To develop a flame-spreading correlation, it is useful to consider the flame-spreading time interval. By definition, the dimensionless flame-spreading time interval $\Delta\tau_{FS}$ is defined as the time measured from the onset of the flame-spreading event t_1 to the end of the flame-spreading event t_2, divided by a reference time selected as the flow residence time t_{res}. These equations are given as follows:

$$\Delta\tau_{FS} \equiv \frac{(t_2 - t_1)}{t_{res}} \tag{3}$$

$$\text{where } t_{res} \equiv \frac{L_{fin-slot}}{V_{core}} \tag{4}$$

The flow residence time, t_{res}, was defined as the axial length of the fin-slot region divided by the bulk velocity of the core flow gas. To relate the experimental $\Delta\tau_{FS}$ to a calculated $\Delta\tau_{FS}$, the following functional relationship was proposed based upon the observed strong effects of pressurization rate and possible dependency on the average chamber pressure in the fin-slot region during the flame-spreading period

$$\Delta\tau_{FS} = \frac{C}{(\frac{dP^*}{dt^*})^{n_1}(P^*)^{n_2}} \downarrow \tag{5}$$

The term dP^*/dt^* represents the dimensionless pressurization rate during the flame spreading and P^* the dimensionless average pressure (for $t_1 \le t \le t_2$). The relationships between the dimensionless and dimensional quantities are given as follows, using the initial atmospheric pressure as a reference pressure:

$$\frac{dP^*}{dt^*} = \frac{t_{res}}{P_{atm}}\left(\frac{dP}{dt}\right) \tag{6}$$

$$P^* = \frac{(P_1 + P_2)}{2P_{atm}} \tag{7}$$

The combined photodetector and high-speed digital camera data were used to determine the experimental $\Delta\tau_{FS}$ based upon the ignition delays observed in tests 1–8. A multiregression analysis led to the development of the following correlation with dP^*/dt^* as the only independent parameter, even though the average pressure was considered in Eq. (5):

$$\Delta\tau_{FS} = \frac{28.04}{(\frac{dP^*}{dt^*})^{0.621}} \tag{8}$$

This functional form was based upon Eq. (5) and the constants determined by the multiregression analysis. For the dimensionless flame-spreading interval, it turned out that the value for n_2 in Eq. (5) was very small compared with n_1 ($n_2 < 0.005$). Based on this knowledge, the influence of the average pressure on the flame spreading was neglected.

A comparison between the experimental and correlated flame-spreading interval can be seen in Fig. 10. It was observed that the experimental results agreed very well with the correlated results, with nearly all of the data falling within $\pm 5\%$ of the correlated results. Even though the correlation for this head-end fin-slot motor had good agreement, application of this correlation for other rocket motor geometries and propellants must be used with caution, because the pressurization rate will be influenced by these parameters.

From the results and data analysis of the eight fin-slot test firings, it was determined that the fin-slot region pressurization rate has the greatest influence on the overall flame-spreading interval. Physically, this meant that the transient phenomena of flame spreading into the fin-slot region were controlled by the hot gas penetration and the recirculating flow processes in the fin-slot region. The higher the pressurization rate, the greater the hot product gas interaction with the unburnt propellant surface, creating a higher heat feedback to the propellant surface, resulting in a shorter flame-spreading time interval.

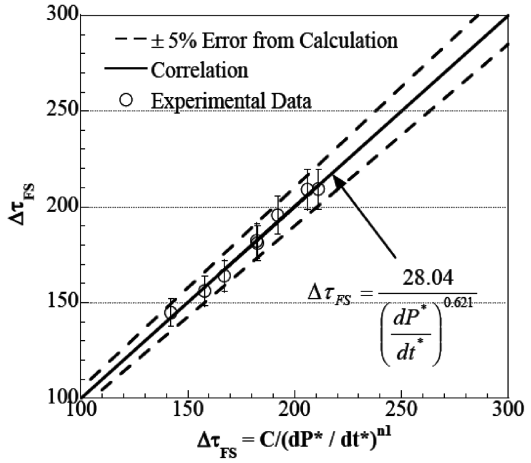

Fig. 10 Comparison of flame-spreading correlation with experimental data.

V. Conclusion

A 1:10 scale RSRM head-end fin-slot motor was designed and fabricated to study the internal flowfield, heat-transfer, and flame-spreading phenomena across the propellant surface. Eight fin-slot propellant experiments were conducted with a variety of diagnostic measurements that included photodetectors, exposed fine-wire thermocouples, and high-speed movie films. The major findings from this fin-slot flame-spreading study include detection of flame-spreading phenomena using visualization and photodetector diagnostic measurements, the development of a flame-spreading time interval correlation as a function of pressurization rate, and demonstrated that the higher the pressurization rate, the lower the flame-spreading interval. The detailed conclusions are described next.

1) A dimensionless correlation was developed showing the relationship between the local chamber pressurization rate and overall flame-spreading time interval. It was found that the flame-spreading time interval is inversely proportional to the local fin-slot pressurization rates to the power of about 0.62.

2) The greater the pressurization rate, the shorter the flame-spreading time interval. The average flame-spreading rate in the fin-slot region was found to be substantially lower than those rates in the circular-bore propellant segments (3.5 to 5.0 m/s $\ll 100's$ m/s). This is why the flame-spreading process in the fin-slot region has a controlling effect on the overall ignition transient phenomena in the segmented RSRM.

3) A highly nonuniform flame-spreading process was observed experimentally.

4) The propellant surface first ignited somewhere in the downstream section of the fin-slot region and also at the location where the igniter induced flow impinged on the upper edge of the fin-slot propellant. The flame fronts in these two regions then merged and burnt propellant front propagated upstream toward the igniter end of the fin-slot region, ending somewhere along the curved contour of the fin-slot region.

Acknowledgments

The authors would like to acknowledge the support and encouragement of James Braithwaite of ATK-Launch Systems and Daryl Woods of NASA for this research work conducted at the Pennsylvania State University through a subcontract funded through Ray Pawlicki's office at Armament Research, Development and Engineering Center of the U.S. Army under the contract of DAAE30-00-9-0813. We would also like to thank Jonathan Janssen, Timothy Kibbey, Robert Lundgreen, Ounyoung Park, Brent Wiesenberg, Bill Dunn, and Mart Cook of ATK-Launch Systems for their input in our 1/10 motor simulator design of the first segment of the RSRM, igniter propellant firing simulations, and propellant sample casting and shipment. Special thanks to R. Brian Wehrman of Pennsylvania State University for his initial setup work and igniter testing of the fin-slot motor. We would also like to thank Ryan Houim of Pennsylvania State University for his help in initial CFD simulation.

References

[1] Kumar, M., and Kuo, K. K., "Flame Spreading and Overall Ignition Transient," *Fundamentals of Solid Propellant Combustion*, edited by K. K. Kuo, and M. Summerfield, AIAA, New York, Vol. 90, 1984, pp. 305–360.

[2] Most, W. J., Parker, K. H., and Summerfield, M., "The Ignition Transient in Solid Propellant Rocket Motors," *2nd AIAA/ASME/SAE/ASEE Joint Propulsion Conference and Exhibit*, AIAA Paper 1966-666, 1966.

[3] Mitchell, R. C., and Ryan, N. W., "Flame Spread on Solid Propellant," *Journal of Spacecraft and Rockets*, Vol. 2, No. 4, 1965, pp. 610–612. doi:10.2514/3.28243

[4] Peretz, A., Kuo, K. K., Caveny, L. H., and Summerfield, M., "Starting Transient of Solid-Propellant Rocket Motors with High Internal Gas Velocities," *AIAA Journal*, Vol. 11, No. 12, 1973, pp. 1719–1727. doi:10.2514/3.50676

[5] Johnston, W. A., "Solid Rocket Motor Internal Flow During Ignition," *Journal of Propulsion and Power*, Vol. 11, No. 3, 1995, pp. 489–496. doi:10.2514/3.23869

[6] Chaouat, B., "Flow Analysis of a Solid Propellant Rocket Motor with Aft Fins," *Journal of Propulsion and Power*, Vol. 13, No. 2, 1997, pp. 194–196. doi:10.2514/2.5169

[7] Kuo, K. K., Kokal, R. A., Paulauskas, M., and Alaksin, P., "Flame-Spreading Phenomena in Fin Slots of a Solid Rocket Motor," *Journal of Propulsion and Power*, Vol. 17, No. 5, 2001, pp. 1005–1011. doi:10.2514/2.5862

[8] Ciucci, A., Jenkins, R. M., and Foster, W. A., Jr., "Analysis of Ignition and Flame Spreading in Solid Rocket Motor Star Slots," *Journal of Propulsion and Power*, Vol. 11, No. 6, 1995, pp. 1371–1373. doi:10.2514/3.51447

[9] Sutton, G. P., and Biblarz, O., *Rocket Propulsion Elements*, 7th ed., Wiley, New York, 2001, pp. 48–96 and 544–545.

[10] Timnat, Y. M., *Advanced Chemical Rocket Propulsion*, Academic Press, New York, 1987, pp. 197–214.

[11] Gatland, K., *Space Technology*, Salamander Books, Ltd., New York, 1981, pp. 198–213.

[12] Caveny, L. H., Kuo, K. K., and Shackelford, B. W., "Thrust and Ignition Transients of the Space Shuttle Solid Rocket Motor," *Journal of Spacecraft and Rockets*, Vol. 17, No. 6, 1980, pp. 489–494. doi:10.2514/3.28041

[13] Parker, K. H., Wenograd, J., and Summerfield, M., "The Ignition Transient in Solid Propellant Rocket Motors," *Solid Propellant Rocket Conference*, AIAA Paper 1964-126, 1964.

[14] McAlevy, R. F., III., Magee, R. S., Wrubel, J. A., and Horowitz, F. A., "Flame Spreading over the Surface of Igniting Solid Rocket Propellants and Propellant Ingredients," *AIAA Journal*, Vol. 5, No. 2, 1967, pp. 265–271. doi:10.2514/3.3951

[15] Kulkarni, A. K., Kumar, M., and Kuo, K. K., "Review of Solid-Propellant Ignition Studies," *AIAA Journal*, Vol. 20, No. 2, 1982, pp. 243–244. doi:10.2514/3.51071; also *16th AIAA/ASME/SAE/ASEE Joint Propulsion Conference and Exhibit*, AIAA Paper 1980-1210, 1980.

[16] Moore, J. D., Ferrara, P. J., Wehrman, R. B., and Kuo, K. K., "Internal Flow Field Structure in a Simulated Fin-Slot Rocket Motor," *41st AIAA/ASME/SAE/ASEE Joint Propulsion Conference and Exhibit*, AIAA Paper 2005-3955, 2005.

[17] Moore, J. D., Wehrman, R. B., Ferrara, P. J., and Kuo, K. K., "Development of a Correlation Between Internal Flow Field and Heat-Flux Measurements in a Simulated Fin-Slot Rocket Motor," *42nd AIAA/ASME/SAE/ASEE Joint Propulsion Conference and Exhibit*, AIAA Paper 2006-4772, 2006.

[18] Thynell, S. T., Huang, I. T., Kuo, C. S., Hiesh, W. H., and Kuo, K. K., "Approach to Measurements of Flame Spreading Over Solid Propellants," *Journal of Propulsion and Power*, Vol. 8, No. 4, 1992, pp. 914–917. doi:10.2514/3.23571

[19] Price, E. W., Bradley, H. H., Jr., Dehority, G. L., and Ibiricu, M. M., "Theory of Ignition of Solid Propellants," *AIAA Journal*, Vol. 4, No. 7, 1966, pp. 1154–1181.

K. Frendi
Associate Editor